NeuroImage: Clinical 23 (2019) 101850

Contents lists available at ScienceDirect

NeuroImage: Clinical

journal homepage: www.elsevier.com/locate/ynicl

A comparison of resting state functional magnetic resonance imaging to invasive electrocortical stimulation for sensorimotor mapping in pediatric patients

Jarod L. Roland[a,*], Carl D. Hacker[a], Abraham Z. Snyder[b,c], Joshua S. Shimony[b], John M. Zempel[c], David D. Limbrick[a], Matthew D. Smyth[a], Eric C. Leuthardt[a,d,e,f,g,h]

[a] Department of Neurological Surgery, Washington University in St. Louis, St. Louis, MO, United States of America
[b] Mallinckrodt Institute Radiology, Washington University in St. Louis, St. Louis, MO, United States of America
[c] Neurology, Washington University in St. Louis, St. Louis, MO, United States of America
[d] Biomedical Engineering, Washington University in St. Louis, St. Louis, MO, United States of America
[e] Neuroscience, Washington University in St. Louis, St. Louis, MO, United States of America
[f] Mechanical Engineering and Materials Science, Washington University in St. Louis, St. Louis, MO, United States of America
[g] Center for Innovation in Neuroscience and Technology, Washington University in St. Louis, St. Louis, MO, United States of America
[h] Brain Laser Center, Washington University in St. Louis, St. Louis, MO, United States of America

ARTICLE INFO

Keywords:
Resting state
Functional MRI
Mapping
Pediatric
Neurosurgery

ABSTRACT

Localizing neurologic function within the brain remains a significant challenge in clinical neurosurgery. Invasive mapping with direct electrocortical stimulation currently is the clinical gold standard but is impractical in young or cognitively delayed patients who are unable to reliably perform tasks. Resting state functional magnetic resonance imaging non-invasively identifies resting state networks without the need for task performance, hence, is well suited to pediatric patients. We compared sensorimotor network localization by resting state fMRI to cortical stimulation sensory and motor mapping in 16 pediatric patients aged 3.1 to 18.6 years. All had medically refractory epilepsy that required invasive electrographic monitoring and stimulation mapping. The resting state fMRI data were analyzed using a previously trained machine learning classifier that has previously been evaluated in adults. We report comparable functional localization by resting state fMRI compared to stimulation mapping. These results provide strong evidence for the utility of resting state functional imaging in the localization of sensorimotor cortex across a wide range of pediatric patients.

1. Introduction

Mapping eloquent cortex is a common neurosurgical procedure intended to maximize preservation of function. Several mapping modalities exist, but most require invasive diagnostic testing and carry non-trivial risks. The clinical gold standard for functional mapping currently is direct electrical cortical stimulation (ECS) to elicit action or temporarily disrupt function. ECS can be performed intra-operatively using a stimulation probe, or extra-operatively after implantation of electrocorticography (ECoG) surface electrodes. Intra-operative mapping requires awake surgery in the case of language mapping, but may optionally be performed in anesthetized patients for motor mapping.

ECS carries non-trivial risks associated with staged craniotomy in the extra-operative setting, the first stage of which is entirely for diagnostic purposes. Moreover, ECS carries risk of inducing a seizure which can limit adequate diagnostic mapping (Szelenyi et al., 2007). Awake craniotomy is impractical in pediatric patients too young to participate in the awake portion of the procedure. Inability to follow commands and cooperate with the anesthesiologist may lead not only to inadequate mapping, but also significant risk of airway compromise. For these reasons, awake craniotomy in the pediatric population is feasible only in carefully selected, high performing individuals. Asleep intraoperative mapping techniques can also be limited due to the normal neurophysiology of the developing brain in very young patients.

Abbreviations: MRI, magnetic resonance imaging; fMRI, functional magnetic resonance imaging; r-fMRI, resting state functional magnetic resonance imaging; t-fMRI, task based functional magnetic resonance imaging; ECoG, electrocorticography; ECS, electrical cortical stimulation; MLP, multilayer perceptron; BOLD, blood oxygen level dependent

* Corresponding author at: One Children's Place, Suite 4s20, St. Louis, MO 63110, United States of America.
E-mail address: RolandJ@wustl.edu (J.L. Roland).

https://doi.org/10.1016/j.nicl.2019.101850
Received 19 January 2019; Received in revised form 21 April 2019; Accepted 2 May 2019
Available online 04 May 2019

Specifically, transcortical motor evoked potentials (MEPs) are significantly less reliable at ages < 5 years (Motomura et al., 2018).

Extra-operative mapping is an alternative that can be achieved in a staged fashion after surgical implantation of ECoG electrodes. The risk of seizure induction remains, but the risks of airway compromise are eliminated. However, this option necessitates two general anesthesia procedures, one for implant and one for explant and possible intervention. The advantage of this paradigm is that extra-operative mapping can be performed in the relative comfort of the patient's bedside where the potential for adequate participation is maximized.

Magnetic resonance imaging (MRI) is a non-invasive method for achieving functional localization. Task based fMRI (t-fMRI) is the traditional technique wherein alternating task and rest epochs induce a functional response. Although it is non-invasive, t-fMRI depends on adequate patient participation, as does awake stimulation mapping, be it intra-operative or at the bedside.

Resting state fMRI (r-fMRI) is an emerging technique for pre-surgical functional localization that does not depend on subject cooperation with task performance, yet can quickly generate functional maps of the whole brain in individual patients (Hacker et al., 2013). Additionally, r-fMRI can be obtained in both awake and sedated patients, for those unable to tolerate the MRI scanner environment, e.g., owing to claustrophobia. Resting state fMRI has been extensively used in basic and clinical neuroscience research (Leuthardt et al., 2018; Rosazza et al., 2014, 2018; Snyder, 2015). Such studies historically have focused largely on group-level differences between study and control populations, but more recently have obtained meaningful results at the single subject level (Gordon et al., 2017; Hacker et al., 2013; Laumann et al., 2015).

To achieve single subject level r-fMRI analysis, we chose to use a previously reported machine learning approach to mapping individual subject networks (Hacker et al., 2013). This technique applies a classical artificial neural network known as the multilayer perceptron (MLP) for classification of 7 canonical RSNs. Previous applications of this method have been reported comparing adult subjects undergoing either awake surgery or extra-operative mapping (Mitchell et al., 2013) as well as a cohort of patients with brain tumors (Dierker et al., 2017). The output of the MLP is a pseudo-probability score indicating the likelihood of a given voxel belonging to the respective network. A simple threshold applied to this output yields a binary RSN map for the respective network. In this study, we evaluated performance across the full range of MLP scores as well as a systematically determined threshold for a binary RSN map. The precise threshold used is relatively arbitrary, may be cohort specific, and may not translate to other implementations or techniques. Yet, it provides for a consistent measure of performance across individuals and may be optimized for desired goals in a clinical setting. This approach also allows for automated processing such that it may be incorporated in a clinical workflow and integrated with surgical navigation (Leuthardt et al., 2018).

To advance the field of pre-surgical mapping, we assessed the ability of r-fMRI to identify the sensorimotor network in pediatric patients and compared the results to invasive ECS mapping performed at the bedside after ECoG implantation. Our data show comparable r-fMRI versus invasive stimulation mapping results. These data support r-fMRI as an adjunct to pre-operative planning, either to focus subsequent invasive mapping, or potentially as a means of entirely obviating the need for invasive mapping in appropriately selective cases.

2. Methods

Pediatric patients with medically refractory epilepsy undergoing ECoG implant for diagnostic mapping were retrospectively identified in our clinical database. We included patients who had all required data for this analysis, including pre-operative high-resolution structural imaging, pre-operative resting state imaging, post-operative imaging for electrode localization, and bedside stimulation mapping records that clearly identify sensory and/or motor positive electrode sites. Pre- and post-operative imaging data were retrieved including pre-operative MRI and post-operative radiograph and computed tomography (CT). Patient information was retrieved from clinical records including age, sex, side of ECoG implant, sedation requirement for pre-operative imaging, and stimulation mapping notes. Patient selection, surgical candidacy, and ECoG monitoring plan were all determined per clinical criteria alone without regard to research considerations.

Surgical procedures were performed in two stages, with ECoG implant in the first stage, followed by bedside mapping, then electrode explant and possible resection in a planned second stage. The treating neurosurgeon and epileptologist selected the electrode implant location to cover the site of suspected seizure onset zone (SOZ) and adjacent eloquent cortex. ECoG implants consisted of at least one grid and potentially several strips according to an a-priori seizure monitoring plan tailored to each individual.

We used post-implant CT imaging to localize ECoG implants on cortical surface. In two individuals treated before adoption of routine post-op CT imaging, electrodes were localized on the basis of plain skull radiographs alone. To localize ECoG electrodes we used the iELVis toolbox (Groppe et al., 2017) and the Bioimage software suite version 3.01 (Joshi et al., 2011) (https://medicine.yale.edu/bioimaging/suite/). Where only radiographs were available, we used the Location on Cortex package (Miller et al., 2007).

A significant challenge in localizing ECoG electrodes from post-implantation imaging is the cerebral deformation induced by fluid shifts during surgery and mass effect of the implanted electrodes. To take this effect into account, electrode coordinates from an initial localization were projected to the cortical surface generated from pre-operative high-resolution structural MRI. We used FreeSurfer version 5.3 (Dale et al., 1999; Fischl et al., 2004) for cortical surface reconstruction and parcellation of the pre-operative MRI. We used the FreeSurfer *localGI* option (Schaer et al., 2008) to create a smoothed surface from the pial surface mesh. We then projected electrode coordinates to the smoothed surface using the method described by Dykstra et al. (Dykstra et al., 2012). Briefly, this method employs an energy-minimization algorithm that includes displacement and deformation terms. The deformation is quantified by the change in distance between neighboring electrodes when the respective electrode is projected onto the nearest location of the smoothed cortical surface.

All patients underwent standard high-resolution structural MRI studies in the pre-operative planning stages. During this same session, we also obtained resting state (i.e., task-free) blood oxygen level dependent (BOLD) functional magnetic resonance imaging (fMRI). Structural imaging included a T1 weighted magnetization prepared rapid acquisition gradient echo (MP-RAGE) sequence with repetition time (TR) 2000 ms, echo time (TE) 2.5 ms, flip angle 12°, and voxel size 1.0 × 1.0 × 1.0 mm, and a T2 weighted turbo-spin echo sequence with TR 9000 ms, TE 115 ms, flip angle 120°, and voxel size 1.0 × 1.0 × 2.5 mm. The resting state data were collected with echo planar imaging sequences sensitive to BOLD contrast with TR 2070 ms, TE 25 ms, flip angle 90°, and voxel size 4.0 × 4.0 × 4.0 mm. Two runs of resting state fMRI were acquired yielding a total of 400 frames over ~14 min. All imaging was obtained on a 3 T Siemens Trio scanner.

Several individuals required sedation to tolerate MRI due to young age and cognitive delays related to their disease process. The treating anesthesiologist decided the anesthetic agent of choice and technique for each patient at the time of imaging. All clinical decisions were made by the respective physician without regard for research interests.

Resting state fMRI data pre-processing followed previously published methods using the 4dfp software suite (Shulman et al., 2010) (https://readthedocs.org/projects/4dfp/). In brief, this included correction for slice acquisition, normalization of intensity scale to mode 1000, and correction for head motion between frames, and re-sampling to 3 mm cubic voxels. The time series were low-pass filtered at < 0.1 Hz and spatially smoothed with a 6 mm at full-width half-max Gaussian

kernel. Nuisance variables that were regressed from the signal included parameters derived by rigid body head motion correction, and the BOLD signal from the bilateral lateral ventricles, white matter regions of non-interest, and the global signal. Frame censoring was performed based on the computed temporal derivative of variance (DVARS) calculated after nuisance regression by the root mean-squared frame-to-frame signal change across voxels (Power et al., 2012, 2014). Frames with DVARS > 0.5% were excluded from functional connectivity analyses. Image registration was performed as previously described (Roland et al., 2017) including registration of T2 weighted images to a common atlas space and cross-modal registration of T1 and EPI sequences to the respective T2 weighted image. We combined all transformation matrices in to a single transformation matrix in order to perform atlas transformation and motion correction in a single resampling step.

Next, we analyzed the pre-processed resting state data, using a previously trained, multilayer perceptron (MLP) (Hacker et al., 2013). The MLP is a machine learning algorithm that assigns resting state network (RSN) affiliation to every voxel in the brain. Implementation of the MLP for RSN classification in individual subjects has been previously described in great detail by Hacker et al. (2013). In brief, the algorithm was trained on a large seed-based r-fMRI data set where seeds were selected by meta-analysis of previously published task and resting state fMRI literature. The trained algorithm then takes in pre-processed r-fMRI data and assigns a pseudo-probability of RSN membership on a per voxel basis. The pseudo-probability is a fractional score from 0 to 1 for each RSN. If we assume each voxel belongs to only one RSN, then network assignment may follow a winner-take-all method where the RSN with highest score is assigned to the respective voxel. Alternatively, an individual voxel can be considered as belonging to more than one RSN where the score may be interpreted as strength of assignment. In our analysis, we used the score for the sensorimotor network (SMN) and a minimum threshold score to assign network membership. This technique has previously been compared to direct cortical stimulation mapping in adult neurosurgical patients by Mitchell et al. (2013).

We performed seed-based analysis for one outlier subject to compare the results with the MLP generated output. We used the sensorimotor network seeds described by Hacker et al. to generate an SMN map for each seed and then projected the mean of these maps to the surface for display. This was qualitatively compared to the MLP map to determine if the outlying results were likely present in the acquired data versus a result of mis-classification by the MLP algorithm.

We performed all imaging analysis in a common image space. This allowed for subsequent comparison of stimulation mapping results on a per electrode basis with the nearest underlying voxel and its respective RSN, as determined by the MLP, and the structural parcellation, as determined by FreeSurfer. Fig. 1 presents a schematized high-level overview of the analysis pipeline. After image processing and electrode localization, we imported all data into Matlab version 2015b for further analysis (The MathWorks Inc., Natick, MA).

Using stimulation mapping results as the clinical gold standard, we calculated the true-positive, true-negative, and receiver operating characteristics (ROC) for each individual at varying thresholds of the MLP score for the SMN. We calculated the area-under-the-curve (AUC) and Youden's J statistic for the group mean ROC curve to characterize performance of r-fMRI in localized sensorimotor cortex. Youden's J is a statistic that captures performance of a diagnostic test by maximizing the true-positive and true-negative. We use it to inform our choice of an MLP threshold for SMN assignment.

We plotted the MLP score for the SMN projected on the cortical surface of each individual and overlaid the ECoG electrodes color-coded according to ECS mapping results to visualize this comparison. We also visualized the SMN maps in volume space binarized at the previously determined threshold. By combining the group data into a voxel-based map, we identify areas of common SMN assignment across the group

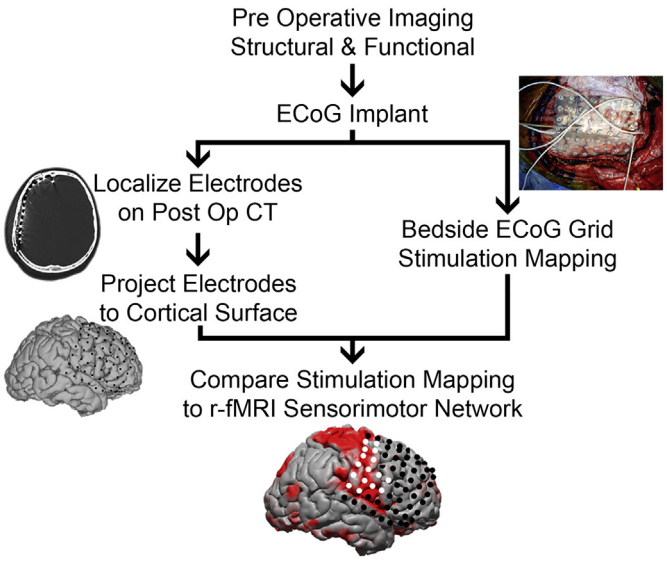

Fig. 1. Methods diagram.
The diagram demonstrates functional imaging analysis proceeding in parallel to clinical mapping and subsequent convergence of results.

and display the results over the pediatric 4.5 to 18.5-year-old MNI atlas symmetric template (Fonov et al., 2011).

Despite ECS being the clinical gold standard, it is subject to error, which may be exacerbated in pediatric patients with varying participation levels during the mapping procedure. For this reason, we also compared the MLP to structural data where sensorimotor function is expected in the pre-central gyrus, post-central gyrus, and para-central gyrus as identified by FreeSurfer parcellation. This structural analysis is similar to that previously reported in adult neurosurgical patients with cerebral tumors by Dierker et al. (2017). We display the structural parcellation and thresholded MLP network assignment for each individual on their respective cortical surfaces as well as the structural parcellation with overlaid electrodes color-coded by ECS results (Fig. 2).

We computed the Dice coefficient to quantify the overlap of MLP network assignment at varying thresholds with the structural parcellation. From these data, we identified the MLP threshold that maximized overlap between the two maps. Structural parcellation is less dependent than ECS on patient participation. Therefore, we compared the max Dice coefficient with age, in scanner movement, and sedation status during r-fMRI to identify systematic bias potentially introduced by these variables. Pearson correlation coefficient and two-sample *t*-test were used for statistical analyses (statistical significance defined as $p < .05$).

Code for these analyses is available online at https://github.com/jarodroland/Peds_rfMRI_vs_ECS. We used code from the Violinplot-Matlab repository available online at https://github.com/bastibe/Violinplot-Matlab. For each subject we created unthresholded MLP maps, which are available online at https://neurovault.org/collections/MBZVNSZY.

3. Results

We identified 16 pediatric patients with data sufficient for the present analysis (Table 1). Ages ranged from 4.0 to 18.6 years-of-age. Grids were located on the right side in 7 and the left in 9 patients. Electrode coverage typically included the lateral convexity with a grid and additional strips where placed as indicated based on pre-operative localization. Only those electrodes included in stimulation mapping, as determined by treating epileptologist on clinical decisions alone, were included for study. Sedation was required to tolerate the MRI scan in 7

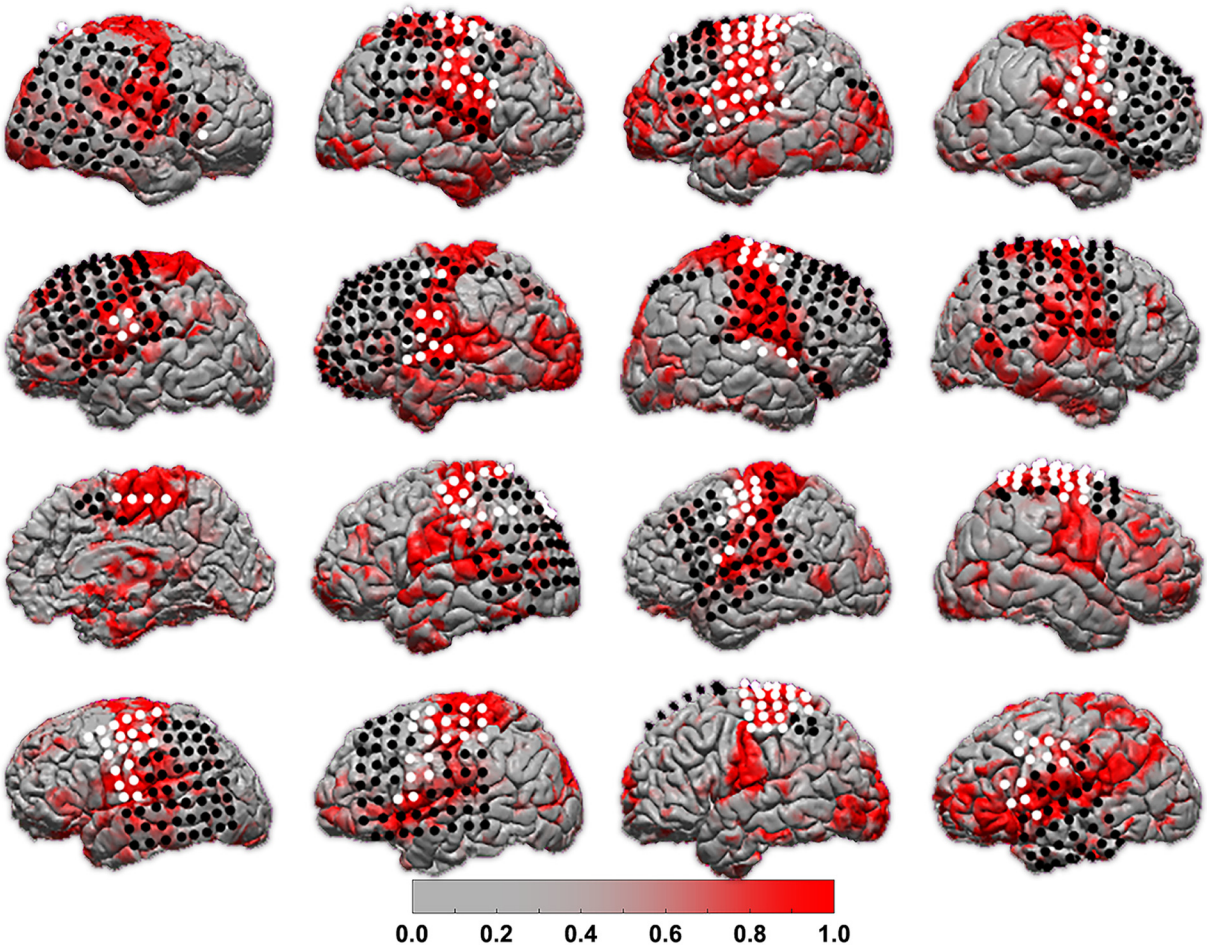

Fig. 2. Individual r-fMRI and ECS mapping.
Each individual's MLP score for the SMN map is projected onto their reconstructed cortical surface. Subjects are organized in row order with Subject A at top left and Subject P at bottom right. ECoG electrodes are color-coded according to positive (white) or negative (black) ECS results for motor and sensory function.

Table 1
Patient demographics.

Subject	Age	Sex	Grid side	Sedated	Age onset
A	4.0	F	Right	Yes	18 mos
B	9.5	M	Right	No	8 yrs
C	12.9	M	Left	No	8 yrs
D	13.4	M	Right	Yes	7 yrs
E	4.8	M	Left	Yes	15 mos
F	12.4	F	Left	No	4 yrs
G	7.3	M	Right	Yes	10 mos
H	3.1	M	Right	Yes	4 mos
I	12.1	F	Right	No	1 yr
J	13.6	F	Left	No	9 yrs
K	18.6	M	Left	No	9 yrs
L	11.9	F	Right	No	5 yrs
M	13.9	M	Left	No	3 yrs
N	9.1	M	Left	Yes	5 yrs
O	17.5	F	Left	No	8 yrs
P	15.0	F	Left	Yes	2 yrs

16 individuals for which r-fMRI and ECS mapping were performed prior to neurosurgical intervention for refractory epilepsy. Age in years.

patients.

In Fig. 2 we show the MLP score for the SMN projected onto each patient's cortical surface. On the cortical surface we overlaid the ECoG electrodes used in ECS mapping and color coded them according to sensory or motor positive (white) or negative (black) results. Visual comparison suggests a correlation between ECS-positive sites with areas of strongest MLP score for the SMN. However, several areas of deviation from expected RSN organization are apparent. For example, some subjects include strong MLP scores over expected anatomy with middle-range scores deviating from expections, such as Subject A, E, and F. The MLP for Subject P is the most notably divergent from expected SMN. To better define the strong signal correlating to sensorimotor cortex from weaker signal attributable to noise, we further compared the varying MLP scores thesholds to the stimulating mapping results.

We then computed the ROC for each individual at varying MLP thresholds. The ROC curves for each individual are displayed in grey lines in Fig. 3. The mean curve is displayed in black and its AUC is shaded grey. The diagonal dashed line represents chance performance. The AUC for the group data is 0.77, suggesting the MLP is a useful tool for identifying sensorimotor cortex. Previously reported reference values describe an AUC of 0.77 as within a “good” (Šimundić, 2008) or “fair test” (Carter et al., 2016) range. The Youden's J statistic identifies a threshold of 0.89 as the MLP score that maximizes true-positive and true-negative results for this group.

Using the threshold identified by ROC analysis, we then combined the binarized SMN maps from all subjects in volume space to create a heat-map of sites most frequently included in the SMN for this group. In Fig. 4, we display this group SMN map at the previously determined threshold over a pediatric template image. Each voxel included in the SMN map of > 2 subjects is shaded according to the total number of subjects whose SMN map included that voxel. This visualization of a resting state network in volume space is familiar to clinicians and can be directly imported to the intra-operative navigation system for an

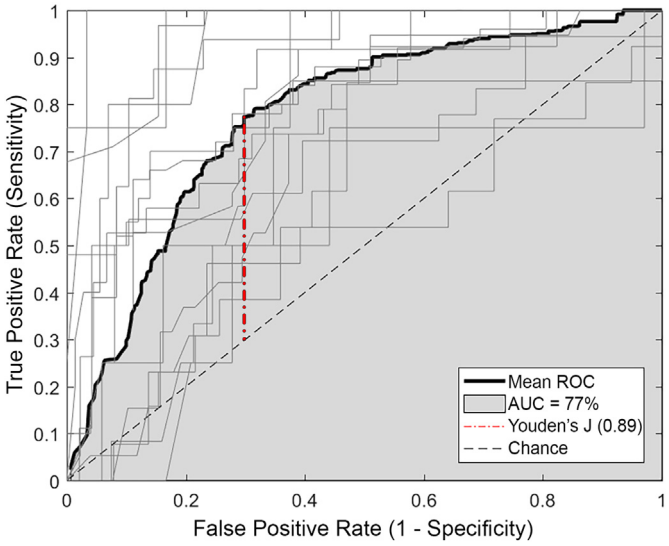

Fig. 3. ROC analysis.
ROC across a range of thresholds for the r-fMRI analysis for each subject shown in light grey and the mean in bold black. AUC for the mean ROC curve is shaded in grey. Youden's J statistic identified with red dash-dot line. Chance performance marked with dashed black diagonal line.

individual subject.

We then displayed the thresholded SMN maps on the cortical surface of each individual in Fig. 5, similar that of the un-threshold data in Fig. 2. In addition, we also displayed the structural parcellation of the pre-central, post-central, and para-central gyrus on the same surface. The SMN map is displayed in red, the structural parcellation in blue, and surface area where the two maps overlap is displayed in green. We then computed the sensitivity and specificity of the functional to anatomic localization across the entire cortical surface. If we assume the anatomic localization to be the ground truth, then the true-positive areas are green, where both anatomic and functional data co-localize, true-negative areas are grey, where neither are present, false-positive areas are red, where the SMN localizes to areas outside of Rolandic cortex, and false-negative areas are blue, where Rolandic cortex is localized but the SMN is not. We computed these statistics for each subject and found a mean sensitivity of 0.51 and specificity of 0.93. The distribution is displayed in violin plots in Supplemental Fig. S1. In Fig. 6 we show the anatomic parcellation with the addition of the electrode coordinates color coded according to ECS results for motor or sensory stimulation positive in white and negative in black.

Of note, Subject P was found to have a very abnormal SMN map as determined by the MLP. We therefore displayed the results of a seed-based analysis in Supplemental Fig. S2 to determine if the source of error reside in the BOLD data or as a result of erroneous classification by the MLP. The seed-based functional map has a similar topography to the MLP determined SMN. This suggests the mis-match with the stimulation mapping is a result of the underlying BOLD data.

The comparison between SMN maps at varying thresholds and the structural parcellation are quantified in Fig. 7 via the Dice overlap coefficient. The curve for each individual is plotted in grey and the mean group data is plotted in black (Fig. 7A). The MLP score that provided the greatest overlap between the SMN map and structural parcellation, as measured by maximum Dice coefficient, is identified by an open circle on each individual's curve. The max Dice coefficient for each individual is correlated to the patient's age (Fig. 7B) and amount of inter-frame movement (Power et al., 2012, 2014) during the r-fMRI scan (Fib 7C). We found no significant relationship with max Dice for age ($r^2 = 0.15, p = .14$) or movement ($r^2 = 0.002, p = .858$). Similarly, we compared the max Dice coefficient for individuals requiring sedation to non-sedated (Fig. 7D) and also found no significant difference.

4. Discussion

Here we demonstrate the r-fMRI for mapping the SMN in a wide age range of pediatric patients who underwent cortical stimulation mapping of sensory and motor cortex. These results show good agreement between the MLP and stimulation mapping, as demonstrated by subjective visual impression in combined plots over the brain surface (Fig. 2) and quantitatively in the ROC analysis (Fig. 3).

Imperfect agreement is partly attributable to uncertainties associated with stimulation mapping (Mandonnet et al., 2010). False-positive ECS results may occur through cortical spread of electrical current leading to activation of distant cortical areas and false localization of function (Borchers et al., 2012). The mechanism may be volume conduction to adjacent areas (Suh et al., 2006) or activity propagation via white matter tracts to distant sites (Ishitobi et al., 2000; Matsumoto et al., 2006). These effects are tempered in practice by starting with a low stimulation current, often 1 mA, and increasing in a step-wise manner until the desired effect is elicited or after-discharges are observed. A step-wise search for current threshold repeated at each site

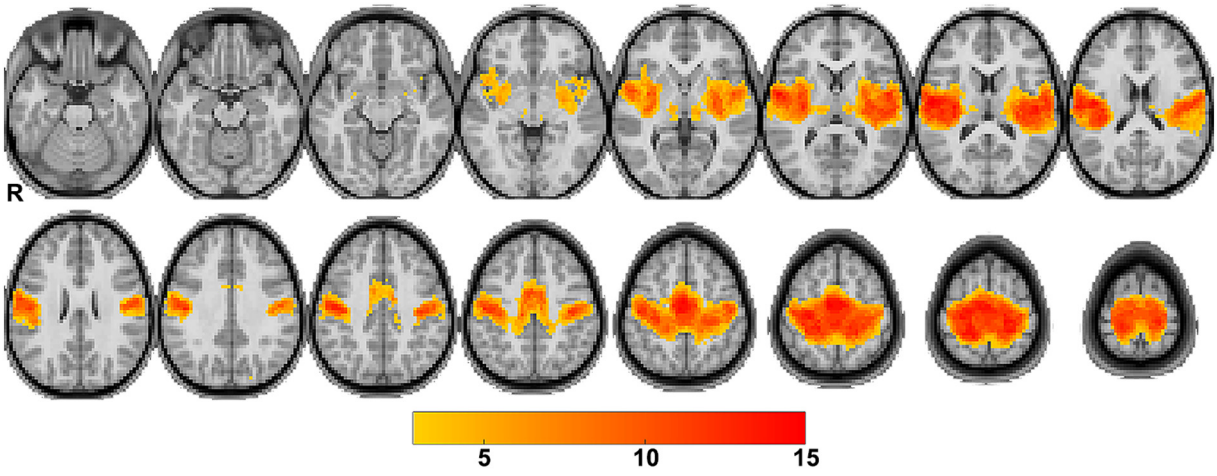

Fig. 4. Group SMN maps.
The SMN maps after threshold applied are plotted on a pediatric representative T1-weighted atlas. Color indicates voxels where the SMN mapped to for > 2 individuals and shows areas of common network localization. (For interpretation of the references to color in this figure legend, the reader is referred to the web version of this article.)

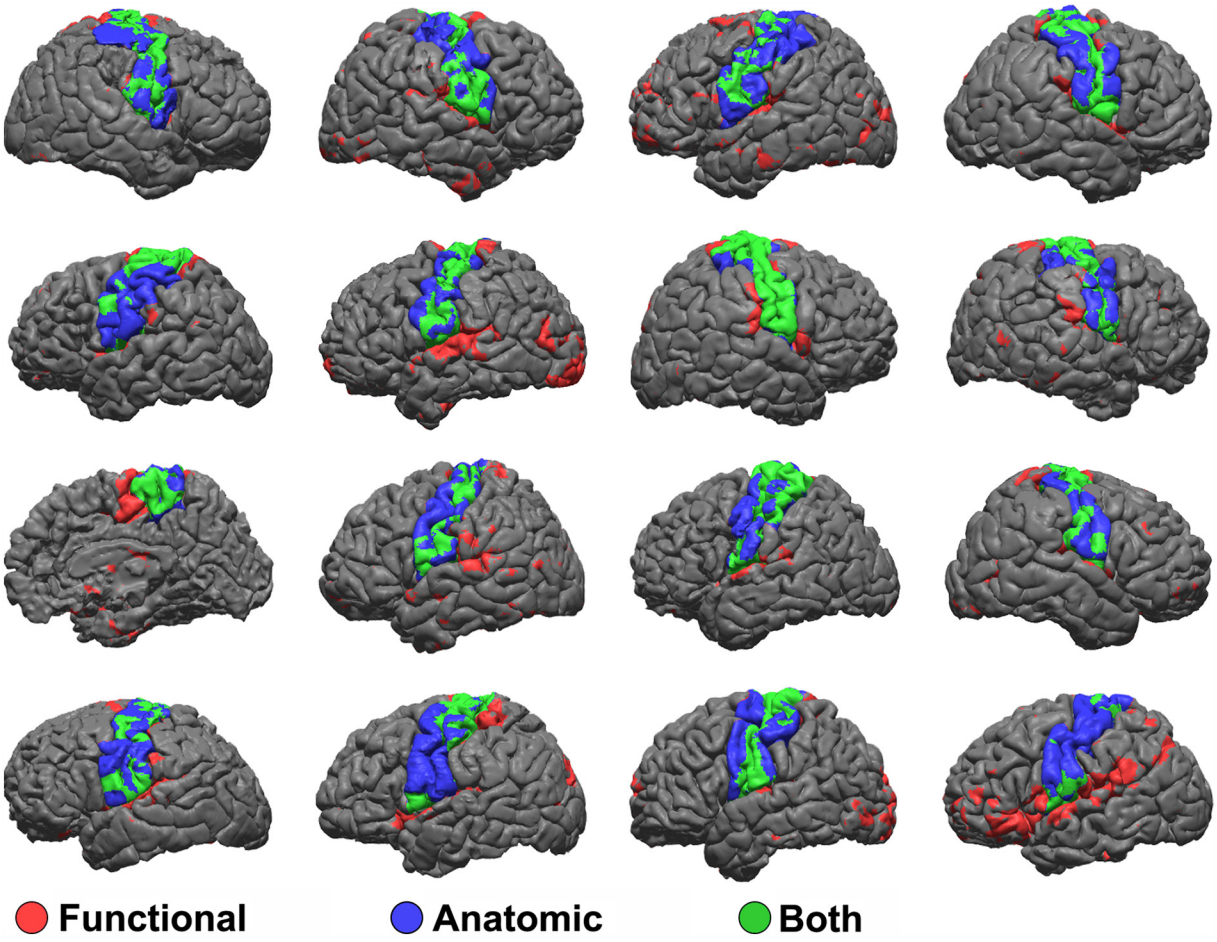

Fig. 5. Functional and anatomic mapping.
Thresholded r-fMRI maps of the SMN are projected onto each individual's cortical surface in red. Anatomic labeling is shown in blue. Common areas where the two maps overlap is shown in green. (For interpretation of the references to color in this figure legend, the reader is referred to the web version of this article.)

can be very time consuming due to the wide range of stimulation response thresholds even within an individual (Corley et al., 2017); an effect may not be elicited until high stimulation current, such as 10 mA or higher. A high threshold may simply be the current necessary at the specific site, or could be the point at which a distant site is activated via current spread leading to a false-positive result.

Beyond the biophysical complexities of ECS, stimulation mapping can be difficult to interpret in pediatric patients. Stringent cooperation during mapping is required so that spontaneous movements are not mis-interpreted as being stimulation induced. Similarly, somatosensory mapping results are dependent on the patient's self-reporting of perceived sensory stimuli. Such reporting may be limited by an individual's level of cognitive development. Therefore, a mapping procedure that is less demanding of a patient's cooperation is uniquely advantageous in pediatric patients.

Other mapping techniques are available and have associated advantages and disadvantages. For young or cognitively immature patients who require sedation to tolerate the MRI environment, passive movement can be performed in a block-paradigm task fMRI study (Ogg et al., 2009). This can be achieved, for example, by a practitioner moving the subject's arm alternating with rest epochs similar to the actions taken by an awake participating subject. The main disadvantage of this technique is the additional personel required to assist with passive motion, but does have the benefit of being non-invasive. Magnetoencephalography (MEG) is an alternative method for functional imaging and can similarly take advantage of passive mapping through the technique of median nerve stimulation during data acquisition (Korvenoja et al., 2006). Unfortunately, MEG is less commonly available compared to MRI and requires additional processing to co-register the data to a familiar imaging space. If the patient is already undergoing craniotomy, then additional passive mapping techniques are available such as median nerve stimulation with simultaneous ECoG monitoring of SSEP phase reversal for localizing the central sulcus (Wood et al., 1988) or slow cortical potential mapping at rest (Breshears et al., 2012). This is necessarily invasive and is not helpful in the pre-operative planning stage.

Given the complexities with ECS mapping mentioned above, we also compared r-fMRI with structural parcellations of sensorimotor cortex, assuming that primary motor and sensory areas localize to the pre-central, post-central, and para-central gyri. This is possible because the patients in our cohort did not have any mass lesions that distort their anatomy and therefore a close structural and functional relationship is reasonable, particularly in the sensorimotor system. Such a comparison would not be feasible for the language network, where the structure-function relationship is more variable.

Resting state fMRI research is a growing at a rapid pace (Snyder, 2015). One of the ongoing challenges regards a robust and accurate analysis methodology, the details of which are beyond the scope of this discussion (for recent review see (Silva et al., 2018)). However, certain methodological traits are relevant to clinical translation. Two canonical methodologies for performing resting state analysis are seed based correlations and independent component analysis (ICA). Seed based correlations require the accurate placement of a seed in an a priori determined functional area in order to discover the extent of the

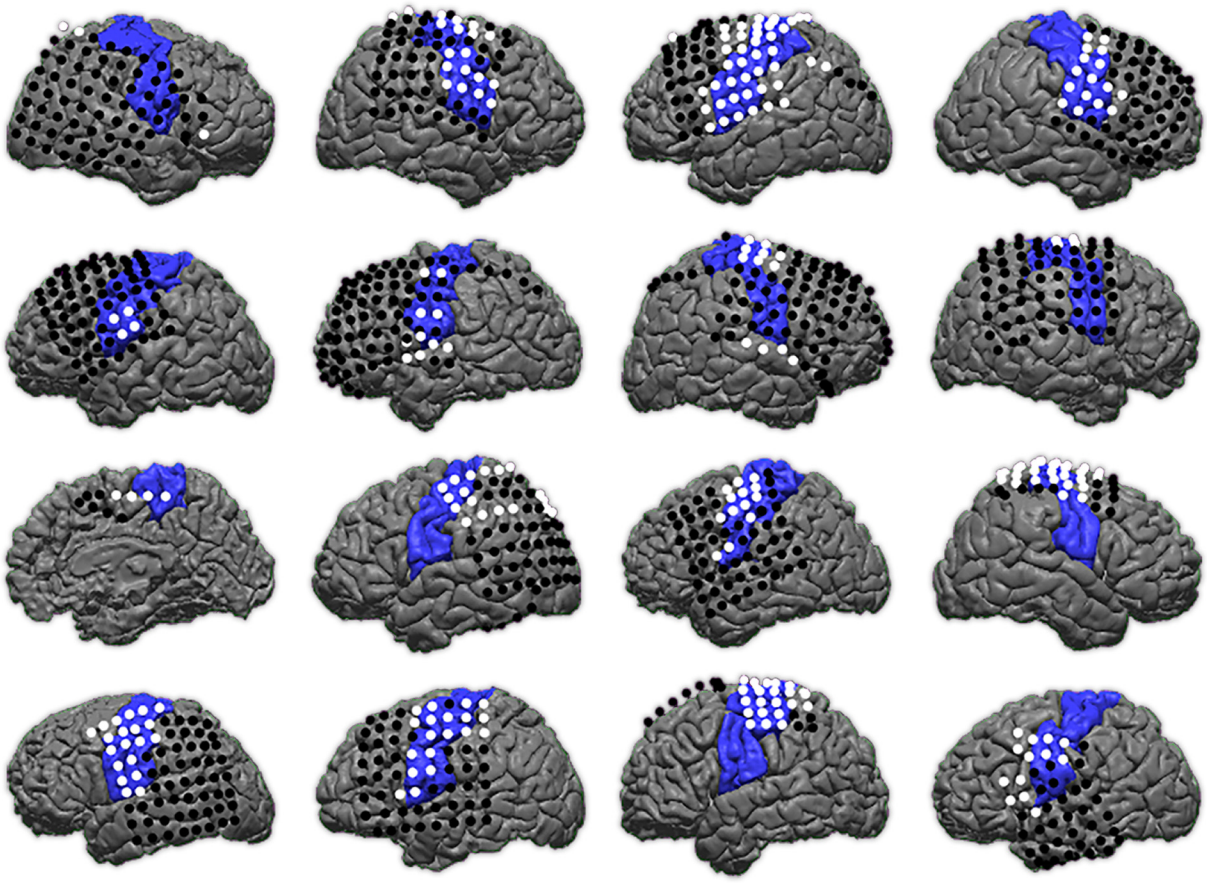

Fig. 6. Anatomic map and ECS results.
Anatomic map of pre-central, post-central, and para-central gyri is shown in blue. ECoG electrodes are overlaid and color-coded for positive (white) and negative (black) ECS motor mapping results. (For interpretation of the references to color in this figure legend, the reader is referred to the web version of this article.)

respective RSN. Seed coordinates are commonly published in the literature and may be used in individuals with normal anatomy. However, the assumption of normal anatomy and typical RSN organization may not hold in many clinical scenarios (Roland et al., 2013). ICA based techniques seek to overcome this limitation by discovering networks in a data driven approach. A trade-off to this approach is that resultant networks must then be labeled by an expert reviewer to identify the RSN of interest. Approaches to match networks discovered by ICA to standard RSN patterns have been reported (Lu et al., 2017; Tie et al., 2014; Zacà et al., 2018), but this procedure re-introduces the assumption of normal RSN organization. Yet another reported alternative begins with a standardized population atlas that is iteratively adapted to the individual subject's data (Wang et al., 2015).

Most individuals in this cohort had similar overlap between r-fMRI, anatomic localization, and stimulation mapping as shown in Fig. 7, with Subject P being the greatest outlier. As previously discussed, the ability of individuals to cooperate is a potential confounding factor that could produce erroneous results. To this end, we compared age, movement during r-fMRI scans, and requirements for sedation to the overlap between the SMN and anatomic localization. None of these variables revealed a significant correlation (Fig. 7B, C, D). Notably, the greatest outlier (Subject P) was not exceptionally young (age 15 yrs) and demonstrated very little motion during r-fMRI (likely attributable to use of sedation). Yet, r-fMRI did not produce a reliable SMN map for this individual, indicating the procedure is not without failure. Despite this, the results were obtained through no effort of the patient and without introducing additional risk. Therefore, despite an unsatisfactory result, it was obtained with little to no cost and all fall back methods for mapping remain available to the neurosurgeon.

This study did have limitations that should be considered when interpreting the results. First, this is a retrospective analysis of previously collected data. Because subject selection is determined entirely by clinical indication and not standardized to a research protocol, the effects of individual traits that could not be controlled for could introduce bias. These effects are common to all retrospective studies. We attempted to identify correlations to certain attributes such as age, movement in the scanner, and requirements for sedation (Fig. 7B–D), but did not detect any such relationship. Our cohort is a relatively small size (16 patients) compared to other larger functional imaging studies. This is due to the highly invasive nature of intracranial electrode recordings in pediatric patients and compares favorably to similar ECoG studies (Mitchell et al., 2013; Rosazza et al., 2014; Zacà et al., 2018; Zhang et al., 2009).

The MLP method we used for r-fMRI analysis classified RSNs to one of seven previously described networks. However, a multitude of network schemes have been described and are varyingly used in the literature. Of particular importance are subnetworks within the SMN. Some RSN parcellations further divide the SMN in to hand (dorsal) and face (ventral) components (Power et al., 2011). There is also a component of the SMN in the operculum and insula that may be attributed to a cinguloopercular network or auditory network in some parcellations (Lee et al., 2012; Power et al., 2011). Therefore, the particular RSN parcellation, and the method for assigning membership to an RSN, may affect the resultant sensitivity and specificity of r-fMRI for identifying sensorimotor cortex. Other authors have similarly investigated methods for automated (Dierker et al., 2017; Lu et al., 2017; Mitchell et al., 2013; Zacà et al., 2018) and semi-automated (Tie et al., 2014) RSN analysis for clinical planning in various patient populations.

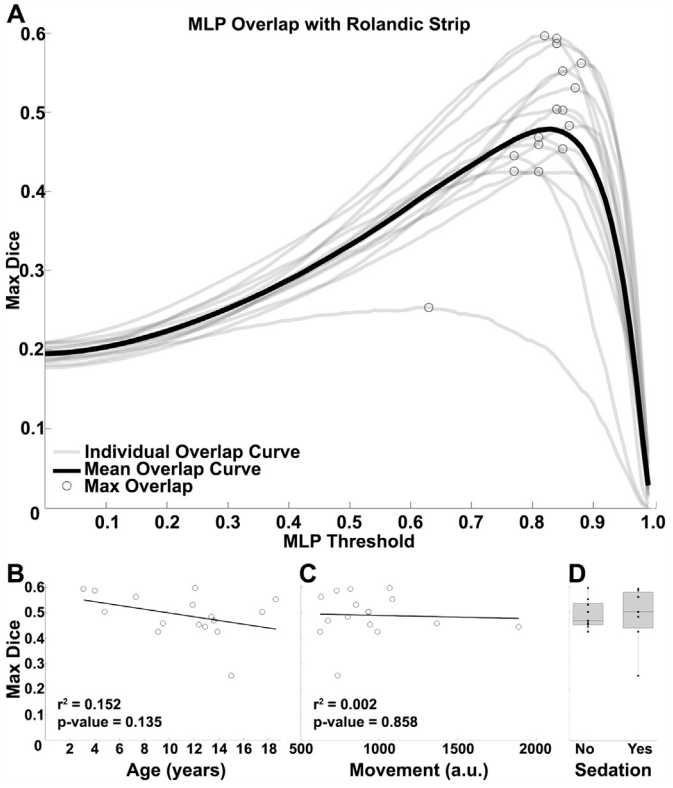

Fig. 7. Comparison of functional and anatomic maps.
(A) Overlap of functional and anatomic maps are evaluated by Dice coefficient across the full range of MLP thresholds and plotted for each individual in grey. The max Dice overlap is identified by open circle. The mean Dice curve is plotted in bold black. The max Dice for each individual is plotted against age (B) and amount of movement during the r-fMRI scan (C), showing no significant correlation for either. (D) The max Dice for each individual grouped by need for sedation during r-fMRI scan is plotted and summarized by box-and-whisker plots where the middle line represents the median, ends of box are 25th and 75th percentiles, and whiskers show the range.

Convergence of methods to a common approach that is thoroughly investigated in the clinical setting will likely optimize this technique in the future.

5. Conclusion

These data provide encouraging results suggesting the feasibility of r-fMRI as a non-invasive adjunct for clinical brain mapping. There are few systematic evaluations of r-fMRI mapping compared to the clinical gold standard of ECS in the literature. Furthermore, despite resting state fMRI being uniquely advantageous in pediatric patients, the majority of reported studies are performed in adult age subjects. These results demonstrate comparable results between r-fMRI and ECS mapping across a wide range of pediatric patients, include sedated and non-sedated, and provide strong support for the successful translation of r-fMRI to clinical practice.

Acknowledgments

Research reported in this manuscript was supported by the National Institutes of Health (NIH) R25-NS090978 grant (JLR), R01-CA203861 grant (ECL & JSS), and the Eunice Kennedy Shriver National Institute of Child Health & Human Development of the NIH under award number U54 HD087011 to the Intellectual and Developmental Disabilities Research Center at Washington University (JSS).

Appendix A. Supplementary data

Supplementary data to this article can be found online at https://doi.org/10.1016/j.nicl.2019.101850.

References

Borchers, S., Himmelbach, M., Logothetis, N., Karnath, H.-O., 2012. Direct electrical stimulation of human cortex — the gold standard for mapping brain functions? Nat. Rev. Neurosci. 13, 63–70. https://doi.org/10.1038/nrn3140.

Breshears, J.D., Gaona, C.M., Roland, J.L., Sharma, M., Bundy, D.T., Shimony, J.S., Rashid, S., Eisenman, L.N., Hogan, R.E., Snyder, A.Z., Leuthardt, E.C., 2012. Mapping sensorimotor cortex with slow cortical potential resting-state networks while awake and under anesthesia. Neurosurgery 71, 305–316. https://doi.org/10.1227/NEU.0b013e318258e5d1.

Carter, J.V., Pan, J., Rai, S.N., Galandiuk, S., 2016. ROC-ing along: evaluation and interpretation of receiver operating characteristic curves. Surgery 159, 1638–1645. https://doi.org/10.1016/J.SURG.2015.12.029.

Corley, J.A., Nazari, P., Rossi, V.J., Kim, N.C., Fogg, L.F., Hoeppner, T.J., Stoub, T.R., Byrne, R.W., 2017. Cortical stimulation parameters for functional mapping. Seizure 45, 36–41. https://doi.org/10.1016/J.SEIZURE.2016.11.015.

Dale, A.M., Fischl, B., Sereno, M.I., 1999. Cortical surface-based analysis: I. segmentation and surface reconstruction. Neuroimage 9, 179–194. https://doi.org/10.1006/NIMG.1998.0395.

Dierker, D., Roland, J.L., Kamran, M., Rutlin, J., Hacker, C.D., Marcus, D.S., Milchenko, M., Miller-Thomas, M.M., Benzinger, T.L., Snyder, A.Z., Leuthardt, E.C., Shimony, J.S., 2017. Resting-state functional magnetic resonance imaging in presurgical functional mapping: sensorimotor localization. Neuroimaging Clin. N. Am. https://doi.org/10.1016/j.nic.2017.06.011.

Dykstra, A.R., Chan, A.M., Quinn, B.T., Zepeda, R., Keller, C.J., Cormier, J., Madsen, J.R., Eskandar, E.N., Cash, S.S., 2012. Individualized localization and cortical surface-based registration of intracranial electrodes. Neuroimage 59, 3563–3570. https://doi.org/10.1016/J.NEUROIMAGE.2011.11.046.

Fischl, B., van der Kouwe, A., Destrieux, C., Halgren, E., Ségonne, F., Salat, D.H., Busa, E., Seidman, L.J., Goldstein, J., Kennedy, D., Caviness, V., Makris, N., Rosen, B., Dale, A.M., 2004. Automatically Parcellating the human cerebral cortex. Cereb. Cortex 14, 11–22. https://doi.org/10.1093/cercor/bhg087.

Fonov, V., Evans, A.C., Botteron, K., Almli, C.R., McKinstry, R.C., Collins, D.L., 2011. Unbiased average age-appropriate atlases for pediatric studies. Neuroimage 54, 313–327. https://doi.org/10.1016/J.NEUROIMAGE.2010.07.033.

Gordon, E.M., Laumann, T.O., Adeyemo, B., Gilmore, A.W., Nelson, S.M., Dosenbach, N.U.F., Petersen, S.E., 2017. Individual-specific features of brain systems identified with resting state functional correlations. Neuroimage 146, 918–939. https://doi.org/10.1016/J.NEUROIMAGE.2016.08.032.

Groppe, D.M., Bickel, S., Dykstra, A.R., Wang, X., Mégevand, P., Mercier, M.R., Lado, F.A., Mehta, A.D., Honey, C.J., 2017. iELVis: an open source MATLAB toolbox for localizing and visualizing human intracranial electrode data. J. Neurosci. Methods 281, 40–48. https://doi.org/10.1016/J.JNEUMETH.2017.01.022.

Hacker, C.D., Laumann, T.O., Szrama, N.P., Baldassarre, A., Snyder, A.Z., Leuthardt, E.C., Corbetta, M., 2013. Resting state network estimation in individual subjects. Neuroimage 82, 616–633. https://doi.org/10.1016/j.neuroimage.2013.05.108.

Ishitobi, M., Nakasato, N., Suzuki, K., Nagamatsu, K., Shamoto, H., Yoshimoto, T., 2000. Remote discharges in the posterior language area during basal temporal stimulation. Neuroreport 11.

Joshi, A., Scheinost, D., Okuda, H., Belhachemi, D., Murphy, I., Staib, L.H., Papademetris, X., 2011. Unified framework for development, deployment and robust testing of neuroimaging algorithms. Neuroinformatics 9, 69–84. https://doi.org/10.1007/s12021-010-9092-8.

Korvenoja, A., Kirveskari, E., Aronen, H.J., Avikainen, S., Brander, A., Huttunen, J., Ilmoniemi, R.J., Jääskeläinen, J.E., Kovala, T., Mäkelä, J.P., Salli, E., Seppä, M., 2006. Sensorimotor cortex localization: comparison of Magnetoencephalography, functional MR imaging, and intraoperative cortical mapping. Radiology 241, 213–222. https://doi.org/10.1148/radiol.2411050796.

Laumann, T.O., Gordon, E.M., Adeyemo, B., Snyder, A.Z., Joo, S.J., Chen, M.-Y., Gilmore, A.W., McDermott, K.B., Nelson, S.M., Dosenbach, N.U.F., Schlaggar, B.L., Mumford, J.A., Poldrack, R.A., Petersen, S.E., 2015. Functional system and areal organization of a highly sampled individual human brain. Neuron 87, 657–670. https://doi.org/10.1016/J.NEURON.2015.06.037.

Lee, M.H., Hacker, C.D., Snyder, A.Z., Corbetta, M., Zhang, D., Leuthardt, E.C., Shimony, J.S., 2012. Clustering of resting state networks. PLoS One 7, e40370. https://doi.org/10.1371/journal.pone.0040370.

Leuthardt, E.C., Guzman, G., Bandt, S.K., Hacker, C., Vellimana, A.K., Limbrick, D., Milchenko, M., Lamontagne, P., Speidel, B., Roland, J., Michelle, M.-T., Snyder, A.Z., Marcus, D., Shimony, J., Benzinger, T.L.S., 2018. Integration of resting state functional MRI into clinical practice – a large single institution experience. PLoS One 13. https://doi.org/10.1371/journal.pone.0198349.

Lu, J., Zhang, H., Hameed, N.U.F., Zhang, J., Yuan, S., Qiu, T., Shen, D., Wu, J., 2017. An automated method for identifying an independent component analysis-based language-related resting-state network in brain tumor subjects for surgical planning. Sci. Rep. 7, 13769. https://doi.org/10.1038/s41598-017-14248-5.

Mandonnet, E., Winkler, P.A., Duffau, H., 2010. Direct electrical stimulation as an input gate into brain functional networks: principles, advantages and limitations. Acta Neurochir. 152, 185–193. https://doi.org/10.1007/s00701-009-0469-0.

Matsumoto, R., Nair, D.R., LaPresto, E., Bingaman, W., Shibasaki, H., Luders, H.O., 2006.

Functional connectivity in human cortical motor system: a cortico-cortical evoked potential study. Brain 130, 181–197. https://doi.org/10.1093/brain/awl257.
Miller, K.J., Makeig, S., Hebb, A.O., Rao, R.P.N., denNijs, M., Ojemann, J.G., 2007. Cortical electrode localization from X-rays and simple mapping for electrocorticographic research: the "location on cortex" (LOC) package for MATLAB. J. Neurosci. Methods 162, 303–308. https://doi.org/10.1016/J.JNEUMETH.2007.01.019.
Mitchell, T.J., Hacker, C.D., Breshears, J.D., Szrama, N.P.N.P., Sharma, M., Bundy, D.T., Pahwa, M., Corbetta, M., Snyder, A.Z., Shimony, J.S., Leuthardt, E.C., 2013. A novel data-driven approach to preoperative mapping of functional cortex using resting-state functional magnetic resonance imaging. Neurosurgery 73, 969–983. https://doi.org/10.1227/NEU.0000000000000141.
Motomura, K., Sumita, K., Chalise, L., Nishikawa, T., Tanahashi, K., Ohka, F., Aoki, K., Hirano, M., Nakamura, T., Matsushita, T., Wakabayashi, T., Natsume, A., 2018. Characterization of intraoperative motor evoked potential monitoring for surgery of the Pediatric population with brain Tumors. World Neurosurg 119, e1052–e1059. https://doi.org/10.1016/J.WNEU.2018.08.039.
Ogg, R.J., Laningham, F.H., Clarke, D., Einhaus, S., Zou, P., Tobias, M.E., Boop, F.A., 2009. Passive range of motion functional magnetic resonance imaging localizing sensorimotor cortex in sedated children. J. Neurosurg. Pediatr. 4, 317–322.
Power, J.D., Cohen, A.L., Nelson, S.M., Wig, G.S., Barnes, K.A., Church, J.A., Vogel, A.C., Laumann, T.O., Miezin, F.M., Schlaggar, B.L., Petersen, S.E., 2011. Functional network organization of the human brain. Neuron 72, 665–678. https://doi.org/10.1016/J.NEURON.2011.09.006.
Power, J.D., Barnes, K.A., Snyder, A.Z., Schlaggar, B.L., Petersen, S.E., 2012. Spurious but systematic correlations in functional connectivity MRI networks arise from subject motion. Neuroimage 59, 2142–2154. https://doi.org/10.1016/J.NEUROIMAGE.2011.10.018.
Power, J.D., Mitra, A., Laumann, T.O., Snyder, A.Z., Schlaggar, B.L., Petersen, S.E., 2014. Methods to detect, characterize, and remove motion artifact in resting state fMRI. Neuroimage 84, 320–341. https://doi.org/10.1016/J.NEUROIMAGE.2013.08.048.
Roland, J.L., Hacker, C.D., Breshears, J.D., Gaona, C.M., Hogan, R.E., Burton, H., Corbetta, M., Leuthardt, E.C., 2013. Brain mapping in a patient with congenital blindness – a case for multimodal approaches. Front. Hum. Neurosci. 7. https://doi.org/10.3389/fnhum.2013.00431.
Roland, J.L., Snyder, A.Z., Hacker, C.D., Mitra, A., Shimony, J.S., Limbrick, D.D., Raichle, M.E., Smyth, M.D., Leuthardt, E.C., 2017. On the role of the corpus callosum in interhemispheric functional connectivity in humans. Proc. Natl. Acad. Sci. https://doi.org/10.1073/pnas.1707050114. 201707050.
Rosazza, C., Aquino, D., D'Incerti, L., Cordella, R., Andronache, A., Zacà, D., Bruzzone, M.G., Tringali, G., Minati, L., 2014. Preoperative mapping of the sensorimotor cortex: comparative assessment of task-based and resting-state fMRI. PLoS One 9, e98860. https://doi.org/10.1371/journal.pone.0098860.
Rosazza, C., Zacà, D., Bruzzone, M.G., 2018. Pre-surgical brain mapping: to rest or not to rest? Front. Neurol. 9, 520. https://doi.org/10.3389/fneur.2018.00520.
Schaer, M., Cuadra, M.B., Tamarit, L., Lazeyras, F., Eliez, S., Thiran, J.-P., 2008. A surface-based approach to quantify local cortical gyrification. IEEE Trans. Med. Imaging 27, 161–170. https://doi.org/10.1109/TMI.2007.903576.
Shulman, G.L., Pope, D.L.W., Astafiev, S.V., McAvoy, M.P., Snyder, A.Z., Corbetta, M., 2010. Right hemisphere dominance during spatial selective attention and target detection occurs outside the dorsal frontoparietal network. J. Neurosci. 30, 3640–3651.
Silva, M.A., See, A.P., Essayed, W.I., Golby, A.J., Tie, Y., 2018. Challenges and techniques for presurgical brain mapping with functional MRI. NeuroImage Clin 17, 794–803. https://doi.org/10.1016/J.NICL.2017.12.008.
Šimundić, A.-M., 2008. Measures of diagnostic accuracy: basic definitions. Med. Biol. Sci. 22, 61–65.
Snyder, A.Z., 2015. Intrinsic brain activity and resting state networks. In: Neuroscience in the 21st Century, pp. 1–52. https://doi.org/10.1007/978-1-4614-6434-1_133-1.
Suh, M., Bahar, S., Mehta, A.D., Schwartz, T.H., 2006. Blood volume and hemoglobin oxygenation response following electrical stimulation of human cortex. Neuroimage 31, 66–75. https://doi.org/10.1016/J.NEUROIMAGE.2005.11.030.
Szelenyi, A., Joksimovic, B., Seifert, V., 2007. Intraoperative risk of seizures associated with transient direct cortical stimulation in patients with symptomatic epilepsy. J. Clin. Neurophysiol. 24, 39–43. https://doi.org/10.1097/01.wnp.0000237073.70314.f7.
Tie, Y., Rigolo, L., Norton, I.H., Huang, R.Y., Wu, W., Orringer, D., Mukundan, S., Golby, A.J., 2014. Defining language networks from resting-state fMRI for surgical planning-a feasibility study. Hum. Brain Mapp. 35, 1018–1030. https://doi.org/10.1002/hbm.22231.
Wang, D., Buckner, R.L., Fox, M.D., Holt, D.J., Holmes, A.J., Stoecklein, S., Langs, G., Pan, R., Qian, T., Li, K., Baker, J.T., Stufflebeam, S.M., Wang, K., Wang, X., Hong, B., Liu, H., 2015. Parcellating cortical functional networks in individuals. Nat. Neurosci. 18, 1853–1860. https://doi.org/10.1038/nn.4164.
Wood, C.C., Spencer, D.D., Allison, T., McCarthy, G., Williamson, P.D., Goff, W.R., 1988. Localization of human sensorimotor cortex during surgery by cortical surface recording of somatosensory evoked potentials. J. Neurosurg. 68, 99–111.
Zacà, D., Jovicich, J., Corsini, F., Rozzanigo, U., Chioffi, F., Sarubbo, S., 2018. ReStNeuMap: a tool for automatic extraction of resting state fMRI networks in neurosurgical practice. J. Neurosurg. 1–8 (epub ahead).
Zhang, D., Johnston, J.M., Fox, M.D., Leuthardt, E.C., Grubb, R.L., Chicoine, M.R., Smyth, M.D., Snyder, A.Z., Raichle, M.E., Shimony, J.S., 2009. Preoperative sensorimotor mapping in brain tumor patients using spontaneous fluctuations in neuronal activity imaged with functional magnetic resonance imaging: initial experience. Neurosurgery 65. https://doi.org/10.1227/01.NEU.0000350868.95634.CA.